Physica C 492 (2013) 21–24

Contents lists available at SciVerse ScienceDirect

Physica C

journal homepage: www.elsevier.com/locate/physc

Normal and superconducting properties of LiFeAs explained in the framework of four-band Eliashberg theory

G.A. Ummarino [a,*], Sara Galasso [a], D. Daghero [a], M. Tortello [a], R.S. Gonnelli [a], A. Sanna [b]

[a] Istituto di Ingegneria e Fisica dei Materiali, Dipartimento di Scienza Applicata e Tecnologia, Politecnico di Torino, Corso Duca degli Abruzzi 24, 10129 Torino, Italy
[b] Max-Planck-Institut für Mikrostrukturphysik, Weinberg 2, D-06120 Halle, Germany

ARTICLE INFO

Article history:
Received 25 March 2013
Received in revised form 3 May 2013
Accepted 7 May 2013
Available online 22 May 2013

Keywords:
Multiband superconductivity
Fe-based superconductors
Eliashberg equations
Non-phononic mechanism
Transport properties

ABSTRACT

In this paper we propose a model to reproduce superconductive and normal properties of the iron pnictide LiFeAs in the framework of the four-band $s\pm$ wave Eliashberg theory. A confirmation of the multiband nature of the system rises from the experimental measurements of the superconductive gaps and resistivity as function of temperature. We found that the most plausible mechanism is the antiferromagnetic spin fluctuation and the estimated values of the total antiferromagnetic spin fluctuation coupling constant in the superconductive and normal state are $\lambda_{tot} = 2.00$ and $\lambda_{tot,tr} = 0.77$ respectively.

Recent ARPES measurements of iron superconductor LiFeAs report four slightly anisotropic gaps [1]. Their isotropic values at 8 K are given by $\Delta_1 = 5.0$ meV, $\Delta_2 = 2.6$ meV, $\Delta_3 = 3.6$ meV, $\Delta_4 = 2.9$ meV and the critical temperature for this compound is $T_c = 18$ K [2]. In another work [3] we disregarded the anisotropic part of the gap values and we tried to reproduce the experimental data in the framework of $s\pm$ wave multiband Eliashberg theory. At first, we calculated [3–8] the Fermi surface, depicted in Fig. 1: five different sheets are present, with two electron pockets centered near the M-point of the Brillouin zone and three hole pockets around the Γ-point. The 5th sheet can be disregarded because of its low density of states and size [3] as can be seen in Table 1. In this way we formulate a four-band s-wave Eliashberg model [9,10] consisting of eight coupled equations for the gaps $\Delta_i(i\omega_n)$ and the renormalization functions $Z_i(i\omega_n)$. If i is the band index (that ranges between 1 and 4) and ω_n are the Matsubara frequencies, the imaginary-axis equations are:

$$\omega_n Z_i(i\omega_n) = \omega_n + \pi T \sum_{m,j} \Lambda^Z_{ij}(i\omega_n, i\omega_m) N^Z_j(i\omega_m) + \sum_j \left[\Gamma_{ij} + \Gamma^M_{ij}\right] N^Z_j(i\omega_n), \quad (1)$$

$$Z_i(i\omega_n)\Delta_i(i\omega_n) = \pi T \sum_{m,j} \left[\Lambda^\Delta_{ij}(i\omega_n, i\omega_m) - \mu^*_{ij}(\omega_c)\right] \times \Theta(\omega_c - |\omega_m|) N^\Delta_j(i\omega_m) + \sum_j \left[\Gamma_{ij} + \Gamma^M_{ij}\right] N^\Delta_j(i\omega_n); \quad (2)$$

where Γ_{ij} and Γ^M_{ij} are the non magnetic and magnetic impurity scattering rates, $\Theta(\omega_c - |\omega_m|)$ is the Heaviside function and ω_c is a cut-off energy. Moreover, $\mu^*_{ij}(\omega_c)$ are the elements of the 4×4 Coulomb pseudopotential matrix and $N^\Delta_j(i\omega_m) = \Delta_j(i\omega_m)/\sqrt{\omega_m^2 + \Delta_j^2(i\omega_m)}$, $N^Z_j(i\omega_m) = \omega_m/\sqrt{\omega_m^2 + \Delta_j^2(i\omega_m)}$. Finally,

$$\Lambda^Z_{ij}(i\omega_n, i\omega_m) = \Lambda^{ph}_{ij}(i\omega_n, i\omega_m) + \Lambda^{sf}_{ij}(i\omega_n, i\omega_m)$$
$$\Lambda^\Delta_{ij}(i\omega_n, i\omega_m) = \Lambda^{ph}_{ij}(i\omega_n, i\omega_m) - \Lambda^{sf}_{ij}(i\omega_n, i\omega_m).$$

Here the superscripts *sf* and *ph* refer to "antiferromagnetic spin fluctuations" and "phonons", respectively. In particular,

$$\Lambda^{ph,sf}_{ij}(i\omega_n, i\omega_m) = 2\int_0^{+\infty} d\Omega \Omega \frac{\alpha^2_{ij} F^{ph,sf}_{ij}(\Omega)}{(\omega_n - \omega_m)^2 + \Omega^2},$$

and the electron–boson coupling constants are defined as

$$\lambda^{ph,sf}_{ij} = 2\int_0^{+\infty} d\Omega \frac{\alpha^2_{ij} F^{ph,sf}_{ij}(\Omega)}{\Omega}. \quad (3)$$

The solution of Eqs. (1) and (2) requires a huge number of input parameters. To make the model solvable, then, it is necessary to

* Corresponding author. Tel.: +39 011 0907313; fax: +39 011 0907399.
E-mail address: giovanni.ummarino@infm.polito.it (G.A. Ummarino).

0921-4534/$ - see front matter © 2013 Elsevier B.V. All rights reserved.
http://dx.doi.org/10.1016/j.physc.2013.05.004

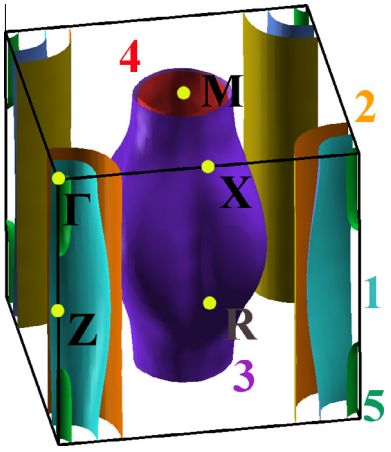

Fig. 1. Fermi surface of LiFeAs [4].

Table 1
Fermi Surface resolved Kohn Sham properties: the Fermi density of states $N(0)$ is given in states/spin/eV and plasma frequencies ω_p in eV. *ab* label the in-plane and *c* for the out-of-plane direction of the diagonals of the plasma tensor [8].

FS	1	2	3	4	5	TOT
$N(0)$	0.556	0.646	0.616	0.370	0.039	2.228
$\omega_p^{\|ab}$	1.131	1.455	1.581	1.161	0.639	2.980
$\omega_p^{\|c}$	0.202	0.034	0.890	0.365	0.319	1.523

introduce some simplifications and approximations, aiming to reproduce only the essential physics of the problem. As for many other pnictides we assumed that [3]: (i) the total electron–phonon coupling constant is small [11]; (ii) spin fluctuations mainly provide interband coupling [12]. This means that we can set $\lambda_{ii}^{ph} = \lambda_{ij}^{ph} = 0, \mu_{ii}^{*}(\omega_c) = \mu_{ij}^{*}(\omega_c) = 0$, i.e. the electron–phonon coupling constant and the Coulomb pseudopotential in first approximation compensate each other and $\lambda_{ii}^{sf} = 0$ (only interband SF coupling) [12]. However, within these assumptions, we were not able to reproduce the observed gap values, and in particular the high value of Δ_1. In order to solve this problem it is necessary to introduce an intraband coupling in the first band ($\lambda_{11} \neq 0$).

The final matrix of the electron–boson coupling constants becomes

$$\lambda_{ij} = \begin{pmatrix} \lambda_{11} & 0 & \lambda_{13} & \lambda_{14} \\ 0 & 0 & \lambda_{23} & \lambda_{24} \\ \lambda_{31} = \lambda_{13} v_{13} & \lambda_{32} = \lambda_{23} v_{23} & 0 & 0 \\ \lambda_{41} = \lambda_{14} v_{14} & \lambda_{42} = \lambda_{24} v_{24} & 0 & 0 \end{pmatrix} \tag{4}$$

where $v_{ij} = N_i(0)/N_j(0)$ and $N_i(0)$ is the normal density of states at the Fermi level for the ith band ($i = 1, 2, 3, 4$). We choose spectral functions with Lorentzian shape [12,14] i.e:

$$\alpha_{ij}^2 F_{ij}(\Omega) = C_{ij}\{L(\Omega + \Omega_{ij}, Y_{ij}) - L(\Omega - \Omega_{ij}, Y_{ij})\} \tag{5}$$

where $L(\Omega \pm \Omega_{ij}, Y_{ij}) = \frac{1}{(\Omega \pm \Omega_{ij})^2 + Y_{ij}^2}$ and C_{ij} are normalization constants, necessary to obtain the proper values of λ_{ij} while Ω_{ij} and Y_{ij} are the peak energies and half-widths of the Lorentzian functions, respectively [12]. In all the calculations we set $\Omega_{ij} = \Omega_{ij}^{sf} = \Omega_0^{sf} = 8$ meV [13], and $Y_{ij} = Y_{ij}^{sf} = \Omega_{ij}^{sf}/2$ [14]. The cut-off energy is $\omega_c = 18\ \Omega_0^{sf}$ and the maximum quasiparticle energy is $\omega_{max} = 21\ \Omega_0^{sf}$. Bandstructure calculations (see Table 1) provide information about the factors v_{ij} that enter the definition of λ_{ij}. Eventually the model contains five free parameters: The coupling constants λ_{13}, λ_{23}, λ_{14}, λ_{24} and λ_{11}. We

Table 2
The experimental data are reported in the first row. The second row concerns the pure intraband case ($\lambda_{ii} = 0.0$) while the third one refers to the case where a large intraband term is present. ($\lambda_{11} = 2.1$). The critical temperatures are given in K and the gap values in meV.

	λ_{11}	λ_{tot}	λ_{13}	λ_{23}	λ_{14}	λ_{24}	Δ_1	Δ_2	Δ_3	Δ_4	T_c
Exper.	–	–	–	–	–	–	5.0	2.6	3.6	2.9	18
Theor.	0.0	1.8	1.78	0.66	0.45	0.52	3.7	2.6	3.6	2.9	15.9
Theor.	2.1	2.0	1.15	0.80	0.45	0.30	5.0	2.6	3.6	2.9	18.6

Table 3
The first and second rows concern the phonon case while the third one concerns the case of the antiferromagnetic spin fluctuation spectral function. The γ_i and Ω_0 are given in meV.

	$\lambda_{tr,tot}$	$\lambda_{tr,3}$	$\lambda_{tr,4}$	γ_1	γ_2	γ_3	γ_4	Ω_0
ph 1 band	0.32	–	–	0.90	–	–	–	–
ph 4 bands	0.14	0.44	0.10	5100	5100	0.65	550	–
sf 4 bands	0.77	1.70	1.70	164	164	4.87	1.52	47

have solved the imaginary-axis Eliashberg Eqs. (1) and (2) (the solution is analytically continued to the real-axis by using the Padé approximant technique) by fixing the free parameters to reproduce the low temperature gap values. The large number of free parameters (five) may suggest that from this procedure is possible to find a large set of solutions that produce the same results. On the contrary, as a matter of fact, the predominantly interband character of the model drastically reduces the number of possible choices. At this point there are no more free parameters. We can calculate the critical temperature that turns out to be very close to experimental one [2]: $T_c^{calc} = 18.6$ K. In Table 2 the obtained results are summarized. The problem with this model is the necessity of a large intraband term λ_{11} in order to give a physical interpretation of the experimental data [3].

We consider the experimental temperature dependent resistivity as measured in Ref. [15], and reported in Fig. 3. Its saturation at high temperature [16] suggests that the presence of several sheets in the Fermi surface also affects the normal state transport properties. While the low temperature behaviour $\rho(T) \propto T^2$ seems to indicate that a non-phononic mechanism plays a relevant role [17].

We tried to fit the data within a one-band model [18,19] (see Eq. (6) with $i = 1$) where the phonon spectrum has been taken from Ref. [20] and the plasma energy has been obtained by first principle calculation (see Table 1). The transport coupling constant and the value of the impurities are considered as free parameters. The obtained values are reported in Table 3, in particular $\lambda_{tr,tot} = 0.32$ which is in agreement with the calculated value of the transport electron–phonon coupling constant [21]. However, as can be seen in Fig. 2, within a one-band model (black dashed line) the experimental data cannot be reproduced.

The phenomenological model [22] proposed to explain saturation at high temperature generally assumes the presence of parallel conductivity channels where one of them has a strong temperature dependence and another one is characterized by a temperature-independent contribution. In the wake of our model for the superconducting state, we propose a multiband model [23,24] to analyze the resistivity data. We will examine two possible mechanisms responsible for resistivity: phonons and antiferromagnetic spin fluctuations. The theoretical expression of resistivity as function of temperature [23,24] is given by the equation:

$$\frac{1}{\rho_c(T)} = \frac{\varepsilon_0}{\hbar} \sum_{i=1}^{4} \frac{(\hbar\omega_{pl,i})^2}{\gamma_i + W_i'(T)}, \tag{6}$$

where $\omega_{pl,i}$ is the bare plasma frequency of the i-band and

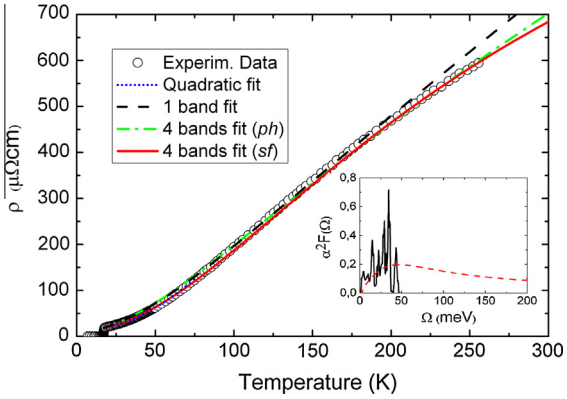

Fig. 2. Temperature dependence of resistivity in LiFeAs. Experimental data (from Ref. [15]) and calculated fits are reported. The black dashed line comes from a single-band model. Within a four-band model two different cases have been considered, one obtained with the phononic spectrum (green dash-dotted line) and one with the antiferromagnetic spin fluctuation spectrum (red solid line). The inset shows the two normalized spectral function that have been used, the phonon spectrum (black solid line) and the antiferromagnetic spin fluctuation spectrum (red dashed line). (For interpretation of the references to colour in this figure legend, the reader is referred to the web version of this article.)

$$W_i'(T) = 4\pi k_B T \int_0^\infty d\Omega \left[\frac{\hbar\Omega/2k_BT}{\sinh(\hbar\Omega/2k_BT)}\right]^2 \frac{\alpha^2_{tr,i}F_{tr,i}(\Omega)}{\Omega}, \quad (7)$$

here $\gamma_i = \sum_{j=1}^4 \Gamma_{ij} + \Gamma_{ij}^M$ is the sum of the inter- and intra-band non magnetic and magnetic impurity scattering rates present in the Eliashberg equations and

$$\alpha^2_{tr,i}F_{tr,i}(\Omega) = \sum_{j=1}^4 \alpha^2_{tr,ij}F_{tr,ij}(\Omega), \quad (8)$$

where $\alpha^2_{tr}(\Omega)F_{tr,ij}(\Omega)$ are the transport spectral functions related to the Eliashberg functions [18].

If a normalized transport spectral function $\alpha^2_{tr}(\Omega)F'_{tr,i}(\Omega)$ is defined, then $\alpha^2_{tr}(\Omega)F_{tr,ij}(\Omega) = \lambda_{tr,ij}\alpha^2_{tr}(\Omega)F'_{tr,ij}(\Omega)$ where the coupling constants are defined as for the standard Eliashberg functions.

In order to build a model as simple as possible, we chose all the normalized transport spectral functions to be equal, then $\alpha^2_{tr}(\Omega)F'_{tr,i}(\Omega) = \lambda_{tr,i}\alpha^2_{tr}(\Omega)F'_{tr}(\Omega)$ where $\lambda_i = \sum_{j=1,..4}\lambda_{ij}$.

It has been shown that, at least for iron pnictides, this model can have a theoretical support [24] depending on the electronic structure of the compound. The basic idea, based on ARPES and de Haas-van Alphen data, is that transport is drawn mainly by the electronic bands and that the hole bands have a weaker mobility [25]. Then the impurities are mostly present in the hole bands and $\gamma_{1,2} \gg \gamma_{3,4}$, while the transport coupling is much higher in bands 3 e 4 and this means that, at least as a first approximation, λ_1 and λ_2 can be fixed to be zero. In this way we will have two contributions almost temperature independent and two which change the slope of the resistivity with the temperature [24].

Let us start with the phononic case. For simplicity we considered all the spectral functions to be proportional to the phonon spectra used also in a previous fit [20]. As mentioned above the transport spectral functions are similar to the standard Eliashberg functions. The main difference is the behavior for $\Omega \to 0$ [18], where the transport function behaves like Ω^4 instead of Ω^2 as in the superconducting state. So the condition $\alpha^2_{tr}(\Omega)F_{tr}(\Omega) \propto \Omega^4$ has been imposed in the range $0 < \Omega < k_BT_D/10$ and then

$$\alpha^2_{tr}(\Omega)F'_{tr}(\Omega) = b_i\Omega^4\vartheta(k_BT_D/10 - \Omega) + c_i\alpha^2_{tr}(\Omega)F''_{tr}(\Omega)\vartheta(\Omega - k_BT_D/10),$$

where $T_D = 240$ K is the Debye temperature [26], the constant b_i and c_i have been fixed by imposing the continuity in $k_B\ T_D/10$ and the normalization. $\alpha^2_{tr}(\Omega)F''_{tr}(\Omega)$ is proportional to the electron–phonon spectral function [20] while $\alpha^2_{tr}(\Omega)F'_{tr}(\Omega)$ is shown in the inset of Fig. 2.

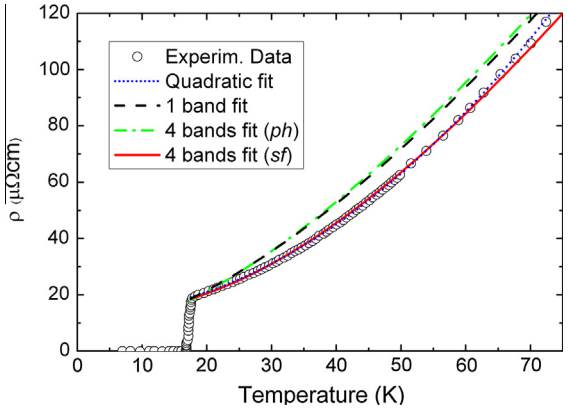

Fig. 3. Magnification of the previous figure. Resistivity at low temperature.

All the plasma frequencies have been determined by first principle calculations (see Table 1) and the coupling constants considered as free parameters as well as the impurities parameters. The best fit is obtained with $\lambda_{tr,tot} = 0.14$, as reported in Table 3, which is in agreement with the hypothesis that the phonon coupling in LiFeAs is very weak and the value of $\lambda_{tr,4}$ almost does not influence the final result. However the experimental data are not perfectly reproduced, as can be seen by looking the green dash-dotted curve in Fig. 2 and in Fig. 3. Moreover a huge quantity of impurity has been necessary to obtain this theoretical curve and this is not consistent with the good quality of the single crystal [16].

Then we considered the case of antiferromagnetic spin fluctuations. Now for $\Omega \to 0$ the transport function behaves like Ω^3 instead of Ω as in the superconducting state. So the condition $\alpha^2_{tr}(\Omega)F_{tr}(\Omega) \propto \Omega^3$ has been imposed in the range $0 < \Omega < \Omega_0/10$, then
$\alpha^2_{tr}(\Omega)F'_{tr}(\Omega) = b_i\Omega^3\vartheta(\Omega_0/10 - \Omega) + c_i\alpha^2_{tr}(\Omega)F''_{tr}(\Omega)\vartheta(\Omega - \Omega_0/10)$ and the constants b_i and c_i have been fixed in the same way as before.

For the spectral function $\alpha^2_{tr}(\Omega)F''_{tr}(\Omega)$ we chose the theoretical antiferromagnetic spin fluctuation function in the normal state [27]

$$\alpha^2_{tr}F''(\Omega) \propto \frac{\Omega_0\Omega}{\Omega^2 + \Omega_0^2}\vartheta(\Omega - \Omega_0), \quad (9)$$

where Ω_0 is a free parameter: from the fit of experimental data we obtain $\Omega_0 = 47$ meV.

Also in this case the value of the free parameters are reported in Table 3 and Fig. 2 depicts the obtained results with the red solid line as well as the spectral function (in the inset).

This approach reproduces accurately the experimental data, significantly better than previous attempts. The fitted total coupling is $\lambda_{tr,tot} = 0.77$ consistent with expectations, and actually smaller than the value in the superconducting state. Moreover the impurity scattering parameters seem to account properly for the high quality of the sample. We are aware that, in spite of the good fitting, this is still a rough simplification as compared to the more plausible situation where the two mechanisms coexist. However, it is clear from our analysis that the antiferromagnetic spin fluctuations must constitute the main contribution.

In conclusion, in this work we have shown that antiferromagnetic spin fluctuations play an important role not only in the superconducting state but also in the normal state, and by fitting the experimental resistivity we have extractedrelevant information on the energy peak of the spectral function and the total transport coupling constant. We also underline the possibility that the very different properties of the mediating boson in the normal and

superconductive state [24] can be a unifying principle at the root of superconductivity in the iron-based materials.

Acknowledgments

We acknowledge the financial support of the European Community through to the Collaborative EU-Japan Project "IRON-SEA" (NMP3-SL-2011-283141).

References

[1] K. Umezawa, Y. Li, H. Miao, K. Nakayama, Z.-H. Liu, P. Richard, T. Sato, J.B. He, D.-M. Wang, G.F. Chen, H. Ding, T. Takahashi, S.-C. Wang, Phys. Rev. Lett. 108 (2012) 037002.
[2] J.H. Tapp, Z. Tang, B. Lv, K. Sasmal, B. Lorenz, P.C.W. Chu, A.M. Guloy, Phys. Rev. B 78 (2008) 060505(R).
[3] G.A. Ummarino, S. Galasso, A. Sanna, J. Phys.: Condens. Matter 25 (2013) 205701.
[4] Electronic structure calculations are done within Kohn-Sham [6] density functional theory in the PBE [5] approximation for the exchange correlation functional and using the experimental lattice structure [2]. Ultrasoft pseudopotentials are used to describe core states, while valence wavefunctions are expanded in planewaves with a 40 Ry cutoff (400 Ry for charge expansion). We use the implementation provided by the ESPRESSO package [7]. A coarse grid of $20 \times 20 \times 16$ k-points is explicitly calculated and then Fourier interpolated to compute accurate Fermi velocities and plasma frequencies.
[5] W. Kohn, L.J. Sham, Phys. Rev. 140 (1965) A1133.
[6] J.P. Perdew, K. Burke, M. Ernzerhof, Phys. Rev. Lett. 77 (1996) 3865.
[7] P. Giannozzi et al., J. Phys. Condens. Matter 21 (2009) 395502.
[8] A.A. Golubov, A. Brinkman, O.V. Dolgov, J. Kortus, O. Jepsen, Phys. Rev. B 66 (2002) 054524.
[9] G.M. Eliashberg, Sov. Phys. JETP 11 (1960) 696.
[10] L. Benfatto, E. Cappelluti, C. Castellani, Phys. Rev. B 80 (2009) 214522.
[11] L. Boeri, M. Calandra, I.I. Mazin, O.V. Dolgov, F. Mauri, Phys. Rev. B 82 (2010) 020506(R).
[12] G.A. Ummarino, M. Tortello, D. Daghero, R.S. Gonnelli, Phys. Rev. B 80 (2009) 172503;
G.A. Ummarino, Phys. Rev. B 83 (2011) 092508.
[13] E.A. Taylor, M.J. Pitcher, R.A. Ewings, T.G. Perring, S.J. Clarke, A.T. Boothroyd, Phys. Rev. B 83 (2011) 220514(R).
[14] D.S. Inosov, J.T. Park, P. Bourges, D.L. Sun, Y. Sidis, A. Schneidewind, K. Hradil, D. Haug, C.T. Lin, B. Keimer, V. Hinkov, Nat. Phys. 6 (2010) 178–181.
[15] O. Heyer, T. Lorenz, V.B. Zabolotnyy, D.V. Evtushinsky, S.V. Borisenko, I. Morozov, L. Harnagea, S. Wurmehl, C. Hess, B. Büchner, Phys. Rev. B 84 (2011) 064512.
[16] S. Kasahara, K. Hashimoto, H. Ikeda, T. Terashima, Y. Matsuda, T. Shibauchi, Phys. Rev. B 85 (2012) 060503(R).
[17] M. Gurvitch, Phys. Rev. Lett. 56 (1986) 647.
[18] P.B. Allen, Phys. Rev. B 17 (1978) 3725–3734.
[19] G. Grimvall, The Electron–Phonon Interaction in Metals, North-Holland, 1981.
[20] A.A. Kordyuk, V.B. Zabolotnyy, D.V. Evtushinsky, T.K. Kim, I.V. Morozov, M.L. Kulić, R. Follath, G. Behr, B. Büchner, S.V. Borisenko, Phys. Rev. B 83 (2011) 134513.
[21] G.Q. Huang, Z.W. Xing, D.Y. Xing, Phys. Rev. B 82 (2010) 014511.
[22] M. Gurvich, Phys. Rev. B 24 (1981) 7404;
Z. Fisk, G.W. Webb, Phys. Rev. Lett. 36 (1976) 1084;
Yu.A. Nefydov, A.M. Shuavaev, M.R. Trunin, Europhys. Lett. 72 (2005) 638.
[23] L. Gozzelino, B. Minetti, G.A. Ummarino, R. Gerbaldo, G. Ghigo, F. Laviano, G. Lopardo, G. Giunchi, E. Perini, E. Mezzetti, Supercond. Sci. Technol. 22 (2009) 065007.
[24] A. A Golubov, O.V. Dolgov, A.V. Boris, A. Charnukha, D.L. Sun, C.T. Lin, A.F. Shevchun, A.V. Korobenko, M.R. Trunin, V.N. Zverev, JETP Lett. 94 (4) (2011) 333–337.
[25] F. Rullier-Albenque, D. Colson, A. Forget, H. Alloul, Phys. Rev. Lett. 109 (2012) 187005.
[26] F. Wei, F. Chen, K. Sasma, B. Lv, Z.J. Tang, Y.Y. Xue, A.M. Guloy, C.W. Chu, Phys. Rev. B 81 (2010) 134527.
[27] P. Popovich, A.V. Boris, O.V. Dolgov, A.A. Golubov, D.L. Sun, C.T. Lin, R.K. Kremer, B. Keimer, Phys. Rev. Lett. 105 (2010) 027003.